ELSEVIER Journal of Materials Processing Technology 47 (1995) 231–249

Journal of Materials Processing Technology

Analysis of cutting forces in ball-end milling

Shiuh-Tarng Chiang, Chung-Min Tsai, An-Chen Lee*

Department of Mechanical Engineering, National Chiao Tung University, 1001 Ta Hsueh Road, Hsinchu 30049, Taiwan

(Received June 8, 1993)

Industrial Summary

A cutting force model for ball end milling is developed, the model being based mainly on the assumption that the cutting force is equal to the product of the cutting area and the specific cutting force. The formulation of the cutting area is derived from the geometry of the mill and the workpiece, whilst the specific cutting force is obtained by third-order curve-fitting of data measured in experiments. The model established in this paper predicts the cutting forces in ball-end milling much more accurately than do previous models.

1. Introduction

Ball-end milling plays an important role in three-dimensional machining, because it has the ability to machine three-dimensional curves easily. While a curved surface is being milled, the tangential cutting speed is minimum (equal to zero) at the tip of the ball, since the rotating radius there is zero, and it is at its maximum value at the periphery of the ball-end mill. When the speed varies along the cutting edge, the related cutting force also changes along the three-dimensional cutting edge. Ball-end milling is thus unlike end milling or face milling, in which the force occurs at the cylindrical periphery of the mill, and it is much more difficult to analyze the force variation in ball-end milling than in these other types of milling. The goal of the present research is to establish a force model to elucidate ball-end milling.

Several studies of end milling have been published [1–3], but studies of ball end milling are few. For the case of full milling, in 1988 Fujii et al. [4] developed a cutting-force model of ball-end milling based on the relationship between the cutting

* Corresponding author.

0924-0136/95/$09.50
SSDI 0924-0136(95)01325-U

area and the specific cutting force, other cases, such as different radial depths of cut and an axial depth of cut greater than the radius of the mill, being left out of their account. In 1991, Yang and Park [5] also presented a cutting-force model of ball-end milling, in their paper the cutting-force model being based on the fundamental mechanics of orthogonal cutting, which assumes that the shear angle, shear stress, and friction angle are functions of cutting speed, feedrate, and normal rake angle, the values of these former three parameters being obtained from turning experiments. However, Yang and Park's theoretical and experimental results do not match very well, because there is a large difference in chip formulation, shear angle, and friction angle between ball-end milling and turning. Hirota and Usui [6] pointed out that the energy dissipation within the chip could not be ignored in larger helix angle cutting, therefore using orthogonal-cutting mechanics to analyze ball-end milling is questionable.

To compensate for the defects of existing models, a new force model is proposed in this paper. In Section 2, a simple and accurate formulation of cutting geometry is proposed based on the method in [4]. In Section 3, a cutting-area model that includes all cutting conditions is developed and a method is presented for calculating the cutting forces of both the ball part and the end-mill part in ball end milling: in the latter operation, not only the ball part but also the end-mill part can machine the workpiece. Existing models deal only with the ball part of ball-end milling, whereas the two parts of the cutter are considered in the present work. Furthermore, in the present work the force model is by considering the effect of the cusp on the workpiece. In end milling, the effect of the cusp is insignificant, but in ball-end milling it is serious. In Section 4, a cutting-force model is proposed based on the product of the cutting area and the specific cutting force, in this model the effect of workpiece hardness being considered: From the point of view of force prediction, it is necessary to study this effect. Finally, in Section 5, a series of experiments performed using various cutting conditions is described, the experimental results for cutting forces verifying the proposed model and showing that it provides consistent results.

2. The cutting edge geometry

2.1. The cutting edge profile

The shape of the edge will affect the outline of the cutting area, i.e. it will affect the cutting force, therefore a full analysis of the silhouette of the edge is the starting point in modeling the cutting-force model. The type of mill studied in this paper is a right-hand screw ball-end mill manufactured by the Nachi Co., the nominal radius of the ball-end mill, the length of the mill, the length of the edge, and the helix angle being 8 mm, 140 mm, 40 mm, and 30°, respectively.

To represent the outline of the edge by a function of coordinates x, y, and z, the origin is defined as being at the center of the ball-end mill. The directions of X, Y, and Z are plotted in Fig. 1. The outline of the edge can be approximated by the

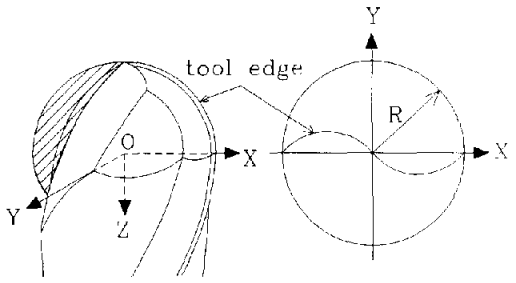

Fig. 1. Cutter geometry and coordinate system for down ball-end milling.

following equations:

$$x = f(t) = Rt$$

$$y = g(t) = -R(a_1 t^4 + a_2 t^3 + a_3 t^2 + a_4 t + a_5), \tag{1}$$

$$z = h(t) = -R(b_1 t^4 + b_2 t^3 + b_3 t^2 + b_4 t + b_5)^{1/2},$$

where R is the nominal radius of the ball nose, t is a parameter that satisfies $0 \leqslant t \leqslant 1$, and a_1–a_5 and b_1–b_5 are constant parameters.

The profile of the edge was measured using a three-dimensional coordinate-measurement machine, the measured data being applied in Eq. (1) and the least-squares method employed to obtain the ten constant parameters listed in Table 1.

2.2. Helix angle and phase difference

The cutting area is located in the contacting position between the edge and workpiece, but the contacting position depends on the phase difference and the helix angle of the above edge position. Therefore, the phase difference and helix angle must be defined clearly in order to be able to derive the cutting area.

The definition of phase difference α is shown in Fig. 2(a). The tangential vector on the top of the ball end ($t = 0$) projected on the O–X–Y plane is defined as $\boldsymbol{q}(0)$, which can be written as $(f'(0), g'(0), 0)$, where the prime denotes the derivation with respect to parameter t. The line from the top point to any position S of the edge projected on to the O–X–Y plane is defined as $\boldsymbol{p}(t)$, which is written as $(f(t), g(t), 0)$. The angle between $\boldsymbol{q}(0)$ and $\boldsymbol{p}(t)$ is the phase difference α of the point S. Thus the phase difference α can be derived by the dot product of $\boldsymbol{q}(0)$ and $\boldsymbol{p}(t)$ or

$$\alpha = \cos^{-1}\left(\frac{\boldsymbol{p}(t)}{|\boldsymbol{p}(t)|} \cdot \frac{\boldsymbol{q}(0)}{|\boldsymbol{q}(0)|}\right)$$

$$= \cos^{-1}\left(\frac{f(t)f'(0) + g(t)g'(0)}{\sqrt{f(t)^2 + g(t)^2}\sqrt{f'(0)^2 + g'(0)^2}}\right). \tag{2}$$

Table 1
Coefficients of the edge profile

$a_1 = -0.73517$	$b_1 = -0.54104$
$a_2 = 0.99551$	$b_2 = 1.363339$
$a_3 = -0.83028$	$b_3 = -1.88824$
$a_4 = 0.63169$	$b_4 = 0.14032$
$a_5 = -0.00494$	$b_5 = 1.00017$

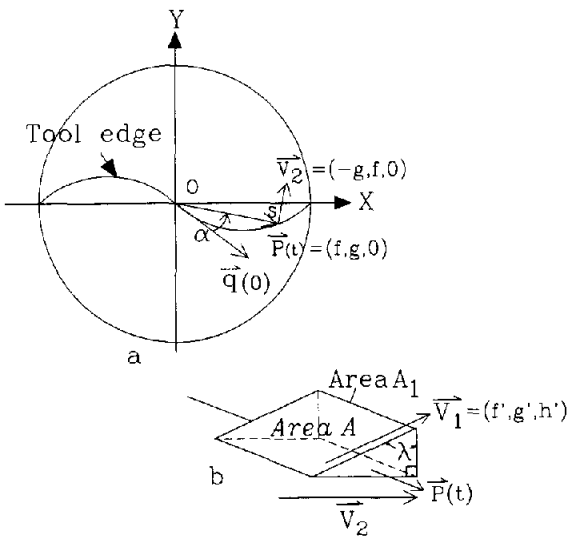

Fig. 2. The definition of phase difference α and helix angle and the relationship between the infinitesimal cutting area A_1 and A.

The definition of the helix angle λ is given in Fig. 2(b), being the angle between the tangential line of the point S and the vertical plane, which is formed by the point S and the central axis of the mill. As shown in Fig. 2(a), vector V_1 is the vector of the tangential line of S and vector V_2 is the normal vector of $p(t)$ in the O–X–Y plane. Thus the helix angle can be determined by the dot product of the vectors V_1 and V_2.

$$\cos\left(\tfrac{\pi}{2} - \lambda\right) = \frac{V_1}{|V_1|} \cdot \frac{V_2}{|V_2|}, \tag{3}$$

$$\lambda = \tfrac{\pi}{2} - \cos^{-1}\left(\frac{-f'(t)g(t) + f(t)g'(t)}{\sqrt{f(t)^2 + g(t)^2}\sqrt{f'(t)^2 + g'(t)^2 + h'(t)^2}}\right). \tag{4}$$

The values of the phase difference α and helix λ angle can be calculated by setting the value of t in Eqs. (2) and (4).

3. Procedures for deriving the cutting area

The cutting area is defined as the product of the chip thickness and the depth of cut. Because the cutting chip thickness is generated by the three dimensional curve of the cutting edge, it is difficult, for example, to determine on what cutting plane it lies, let alone for it to directly represent the cutting area. Therefore, an approximation method is applied that divides the cutting edge into infinitesimal sections. For each section, the related chip thickness and depth of cut are calculated to obtain the cutting area, and then this is substituted into the force model to obtain the infinitesimal cutting force. Finally, the infinitesimal forces are accumulated to obtain the total force.

3.1. The infinitesimal area of the cutting edge on the ball part

The ball-end mill comprises the ball part and the end-mill part. In the ball part, the cutting edge is located on a spherical surface whilst in the end mill part, the edge is located on a cylindric surface. Since the edge shapes of the two parts are different, their cutting behavior and paths are different. In this section is presented a method of calculating the infinitesimal area of the cutting area on the ball part. The following definitions of angles θ, η, and β on the ball end-mill are illustrated in Fig. 3: θ, the angular position of the cutter, is the angle between the vector $\boldsymbol{q}(0)$ and the negative Y axis, the clockwise rotation being defined as positive. η is the angle between the vector V_3 from the origin to the point S and the central axis ($-Z$) of the mill, the value of η being equal to $\sin^{-1}(t)$. β, the engage angle, is the angle between the vector $\boldsymbol{p}(t)$ and the negative Y axis, the counterclockwise rotation being defined as positive.

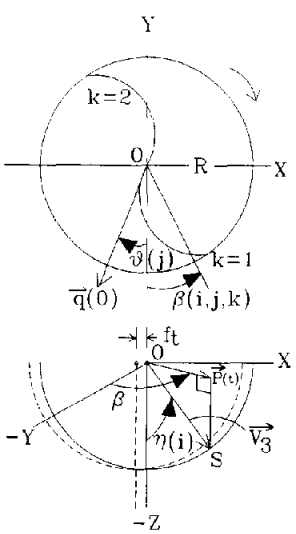

Fig. 3. The definition of angles θ, β, nd η.

In order to describe adequately the position of the infinitesimal cutting area, η is discretized into a small section $\Delta\eta$, whether the ith incremental angle $\eta(i)$ equals $i\,\Delta\eta$, and the total number of sections is N_i. θ is divided into N_j analytical points per cycle, thus the jth rotating angle $\theta(j)$ is $j(2\pi/N_j)$. For a mill with two teeth, the angle between the two teeth is π radians.

The angle β characterizes completely the position of the cutting edge at any given instant. For the right-hand helix mill, α and β have the same direction, therefore the engage angle $\beta(i,j,k)$ can be written as

$$\beta(i,j,k) = -\theta(j) + \alpha(i) + \pi(k-1), \tag{5}$$

where $\alpha(i)$ can be derived by inserting a given value of t, where $t = \sin\eta(i)$, into Eq. (2).

The chip thicknes and cutting area are now expressed with respect to the fixed frame O–X–Y–Z. A simple chip-thickness formulation [1] for milling is $f_t \sin\beta$, were f_t is the feedrate per tooth. In the down ball-end milling shown in Fig. 3, the chip-thickness formulation should be modified. A chip thickness t_c along the η direction for the jth rotating angle and the ith infinitesimal cutting area of the kth tooth can be written as

$$t_c(i,j,k) = f_t \sin\beta(i,j,k)\sin\eta(i), \tag{6}$$

where $\eta(i) = i\,\Delta\eta$. If $\Delta\eta$ is very small, the infinitesimal cutting area projected on the vertical plane can be written as

$$A_1(i,j,k) = t_c(i,j,k)\,R\,\Delta\eta = f_t \sin\beta(i,j,k)\sin\eta(i)\,R\,\Delta\eta. \tag{7}$$

If the effect of helix angle λ is considered, the A_1 obtained has an angle λ with the actual cutting area, as shown in Fig. 2(b). Thus the infinitesimal cutting area A is modified to

$$\begin{aligned} A(i,j,k) &= A_1(i,j,k)\sec\lambda(i) \\ &= f_t \sin\beta(i,j,k)\sin\eta(i)\,R\,\Delta\eta\sec\lambda(i), \end{aligned} \tag{8}$$

where $\lambda(i)$ can be derived by inserting a given value of t into Eq. (4). From Eq. (8), the cutting area increases with parameter λ, i.e., the cutting force for a larger value of angle η is greater than that for a smaller value.

3.2. The infinitesimal cutting area on the end-mill part

If the axial depth of cut A_d is deeper than the ball part, that is $A_d \geqslant R$, Eq. (8) is no longer applicable. To incorporate the effect of the end-mill part, the concept constructed by Kline [3] is employed to obtain the infinitesimal cutting area for end milling. In the end-mill part, the phase difference α in Eq. (5) is modified to

$$\alpha(i) = \alpha_0 + \alpha_e(i), \tag{9}$$

where: α_0 is the phase difference caused by the ball part, which can be obtained by letting $t = 1$ in Eq. (2); and α_e is the phase difference caused by the end-mill part.

N_e is defined as the number of infinitesimal cutting areas of the ball part, in which N_e equals $\pi/(2\Delta\eta)$, the total number of areas for the ball part and end-mill part being N_t. If the ith calculating infinitesimal element, $N_e < i < N_t$, is considered, the infinitesimal cutting area is on the end-mill part. The phase difference α_e is illustrated in Fig. 4. The $\alpha_e(i)$ of the ith disk can be represented in the form

$$\alpha_e(i) = \frac{(i - N_e) D_z \tan \lambda_e}{R}, \tag{10}$$

where D_z is the unit height along the Z axis and λ_e is a constant of the helix angle of the end-mill part.

From Eq. (9) the new phase angle α is substituted into Eq. (5), and the new engage angle β obtained. The infinitesimal cutting area projected onto the vertical cross-section is determined easily as $f_t \sin \beta D_z$. Because the end-mill part has a constant helix angle λ_e, the actual infinitesimal cutting area on the end mill part is described by

$$A(i, j, k) = f_t \sin \beta(i, j, k) D_z \sec \lambda_e. \tag{11}$$

Eq. (11) is an improved model that has less error than that presented by Kline [3]. The term $\sec \lambda_e$ in Eq. (11) can fit the slope of the edge exactly, thus making the present model more precise than Kline's, which approximates the slope of an edge by a saw-tooth.

3.3. Cutting range and cusp effect

The parameters influencing the cutting range of ball-end milling are the axial depth of cut A_d, the radial depth of cut R_d, and the cusps on the workpiece. From Fig. 5, o_1 is an adjacent center of the pre-cut path and o_2 is the current path center with some variation of axial depth of cut δ_{A_d}. In plane cutting, δ_{A_d} is zero, whilst in curvature surface cutting δ_{A_d} is either positive or negative. If it is assumed that the current

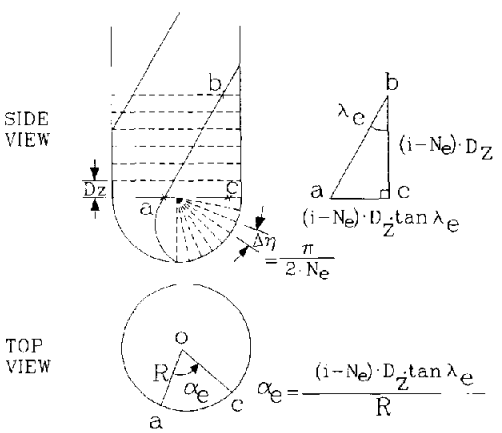

Fig. 4. Discretization of ball-end mill and definition of phase angle of end-mill part.

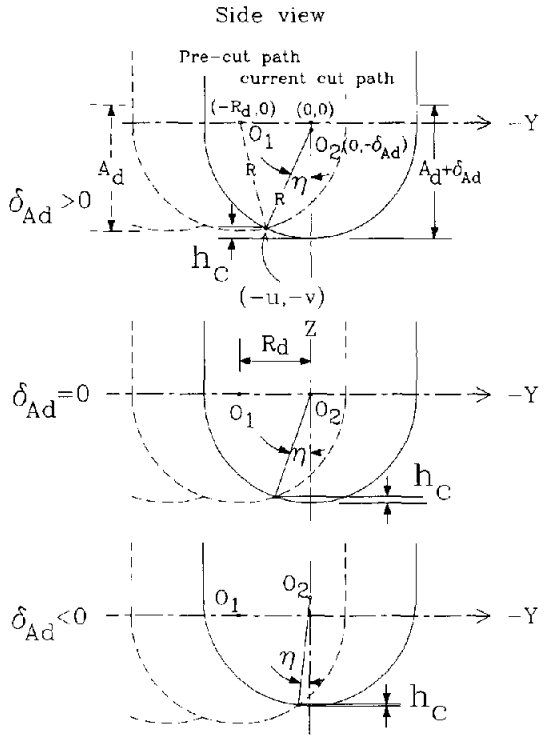

Fig. 5. The cusp height h_c related to variation of depth of cut δ_{Ad}.

position of center o_2 with zero δ_{A_d} is at the original coordinate (0, 0), the intersection point $(-u, -v)$ is the engage line of the current tooth intersected with one of the past cuts. The values of u and v can be obtained from the following relationship:

$$(-u + R_d)^2 + v^2 = R^2,$$

$$u^2 + (-v + \delta_{A_d})^2 = R^2. \tag{12}$$

After the above equation is solved, the current cusp height h_c can be described as follows:

$$h_c = R - \frac{\delta_{A_d}}{2} - \frac{R_d}{2}\sqrt{\frac{4R^2 - R_d^2 - \delta_{A_d}^2}{R_d^2 + \delta_{A_d}^2}}. \tag{13}$$

The value h_c increases when δ_{A_d} goes from positive to negative. The cutting range can be determined accurately by using the value of h_c. Consider the engage angle β in any horizontal cross-section. The cutting range of β is bounded by the exit angle β_{ex} and entry angle β_{en}, i.e.,

$$\beta_{ex} \leqslant \beta(i, j, k) \leqslant \beta_{en}. \tag{14}$$

As described in Fig. 5, it is obvious that if the cutting area is below the cusp height h_c, the cutting process is full milling. In this situation, the entry angle β_{en} is π and the exit angle β_{ex} is zero. When the cutting area is above the cusp height, the value of β_{ex} still equals zero, but the value of β_{en} changes. The formulation of β_{en} can be obtained for various values of $\eta(i)$, i.e., the height of the cutting area, using the following equations:

$$\begin{aligned}
\beta_{en} &= \pi, && \text{case 1, if } R(1-\cos\eta(i)) < h_c \\
&= \cos^{-1}\left(1 - \frac{R_d}{R\sin\eta(i)}\right), && \text{case 2, if } h_c \leqslant R(1-\cos\eta(i)) < R \\
&= \cos^{-1}\left(1 - \frac{R_d}{R}\right), && \text{case 3, if } R \leqslant R(1-\cos\eta(i)).
\end{aligned} \tag{15}$$

Fig. 6 shows the three cases of β_{en} with respect to values of $R(1-\cos\eta(i))$ with zero δ_{A_d}. In case 1, $R(1-\cos\eta(i))$ is smaller than h_c, which means that the cusp is being formed, and β_{en} equals π. In case 2, where $h_c \leqslant R(1-\cos(i)) < R$, the entry angle β_{en} depends on the intersection of the pre-cut boundary and the engage line of current cutting. In case 3, the cutting condition A_d is greater than the normal radius R, i.e., including end milling. It appears that Eq. (15) can deal with typical applications of ball-end milling and it is also suitable for curvature surface milling. A further point is that for case 1, the formulation $\beta_{en} = \cos^{-1}(1-(R_d)/(R\sin\eta(i))$ used by other researchers [4] is not appropriate.

4. Cutting-force model

In this section, the specific cutting forces are defined and an effective method for obtaining these parameters is proposed. Previous papers [3,4] assumed that the specific cutting forces are functions of feed per tooth and not of the workpiece hardness, but in this paper the effect of workpiece hardness on the specific cutting forces is considered.

4.1. Development of cutting-force model

The infinitesimal cutting force acting on the infinitesimal cutting area for the jth rotating angle and ith infinitesimal cutting area of the kth tooth are depicted in Fig. 7, where: $\Delta f_n(i,j,k)$ is the normal force toward the cutting area; $\Delta f_r(i,j,k)$ is the radial force acting from the center point of area $A(i,j,k)$ to the origin of the frame O–X–Y–Z, and $\Delta f_t(i,j,k)$ is the tangential force along the cutting edge. The specific cutting forces in these three directions are K_n, K_r, and K_t, respectively; therefore,

$$\begin{aligned}
\Delta f_n(i,j,k) &= K_n A(i,j,k), \\
\Delta f_r(i,j,k) &= K_r A(i,j,k), \\
\Delta f_t(i,j,k) &= K_t A(i,j,k).
\end{aligned} \tag{16}$$

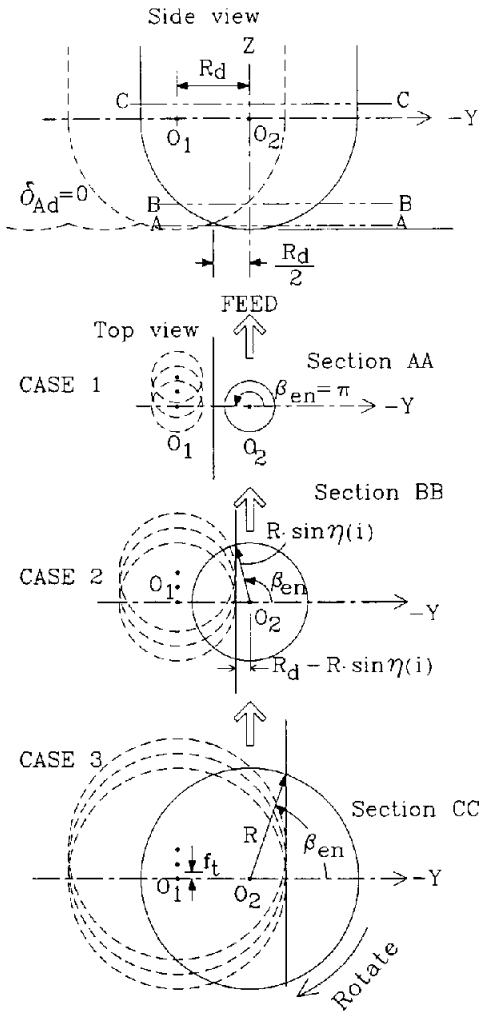

Fig. 6. The cutting range of the ball-end milling.

The cutting forces described in Eq. (16) must be transformed to the global rectangular coordinates X, Y, and Z. The transfer matrices between the local coordinates and the global coordinate are $[T_3]$, $[T_2]$, and $[T_1]$, where

$$[T_1] = \begin{bmatrix} \cos\lambda & 0 & \sin\lambda \\ 0 & 1 & 0 \\ -\sin\lambda & 0 & \cos\lambda \end{bmatrix}, \quad [T_2] = \begin{bmatrix} 1 & 0 & 0 \\ 0 & \cos(\pi/2-\eta) & -\sin(\pi/2-\eta) \\ 0 & \sin(\pi/2-\eta) & \cos(\pi/2-\eta) \end{bmatrix}, \tag{17}$$

$$[T_3] = \begin{bmatrix} \cos\beta & -\sin\beta & 0 \\ \sin\beta & \cos\beta & 0 \\ 0 & 0 & 1 \end{bmatrix}.$$

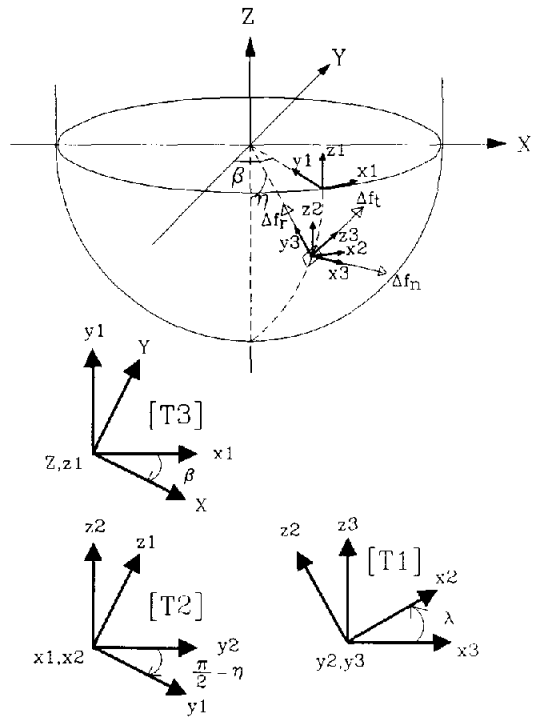

Fig. 7. Illustration of three coordinate rotations of infinitesimal cutting forces Δf_n, Δf_r, and Δf_t.

Thus the relationship between the local and the global cutting forces is

$$\begin{bmatrix} \Delta f_X(i,j,k) \\ \Delta f_Y(i,j,k) \\ \Delta f_Z(i,j,k) \end{bmatrix} = [T_3][T_2][T_1] \begin{bmatrix} \Delta f_n(i,j,k) \\ \Delta f_r(i,j,k) \\ \Delta f_t(i,j,k) \end{bmatrix}. \tag{18}$$

The total cutting forces for the jth rotating angle in the X, Y, and Z directions are the accumulation of the infinitesimal cutting forces, i.e.,

$$\begin{aligned} F_X(j) &= \sum_i \sum_k \Delta f_X(i,j,k), \\ F_Y(j) &= \sum_i \sum_k \Delta f_Y(i,j,k), \\ F_Z(j) &= \sum_i \sum_k \Delta f_Z(i,j,k). \end{aligned} \tag{19}$$

4.2. Determination of the specific cutting forces

The specific cutting forces are the core of the force model. The procedures used to obtain K_n, K_r, and K_t are described in the following. If Eq. (19) is summed for i, j and

k, and each side multiplied by $1/N_j$, then the equation becomes

$$\frac{1}{N_j}\sum_j\sum_i\sum_k\begin{bmatrix}\Delta f_X(i,j,k)\\ \Delta f_Y(i,j,k)\\ \Delta f_Z(i,j,k)\end{bmatrix}=\frac{1}{N_j}\sum_j\sum_i\sum_k[T_3][T_2][T_1]\begin{bmatrix}K_n\\ K_r\\ K_t\end{bmatrix}A(i,j,k), \qquad (20)$$

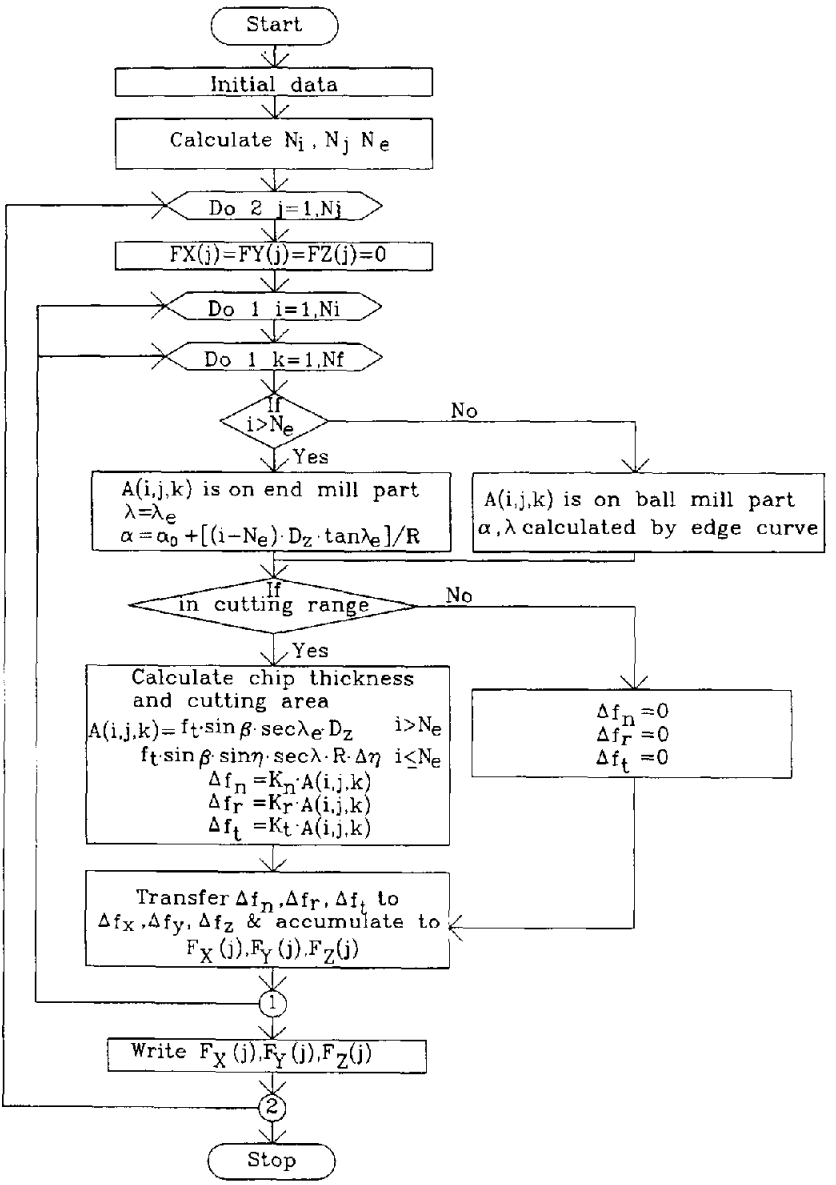

Fig. 8. Flow chart for solving for cutting force.

i.e.,

$$\begin{bmatrix} F_X \\ F_Y \\ F_Z \end{bmatrix} = [T] \begin{bmatrix} K_n \\ K_r \\ K_t \end{bmatrix}, \tag{21}$$

where $[T] = (1/N_j) \sum_j \sum_i \sum_k [T_3][T_2][T_1] A(i,j,k)$. Thus K_n, K_r, and K_t can be induced by the inverse transformation,

$$\begin{bmatrix} K_n \\ K_r \\ K_t \end{bmatrix} = [T]^{-1} \begin{bmatrix} F_X \\ F_Y \\ F_Z \end{bmatrix}, \tag{22}$$

in which $[T]^{-1}$ can be calculated by programs and F_X, F_Y, and F_Z can be measured by experiments.

Using Eq. (22), the specific cutting forces can be obtained from the results of experiment. In previous papers other researchers considered the specific cutting forces to be a function of feed per tooth [1–3] or feed per tooth, rake angle, and cutting velocity [5]. For prediction purposes, the specific cutting forces can be viewed as functions of feed per tooth and workpiece hardness. Because the effects of radial depth of cut and axial depth of cut have been considered in deriving the cutting area, these parameters are no longer considered in the derivation of the specific cutting forces.

A series of tests was performed using different values of feed per tooth f_t and workpiece hardness h_d. Third-order polynomial models were established to evaluate K_n, K_r, and K_t, as below:

$$\begin{aligned} K_n, K_r, K_t = {} & c_1 + c_2 f_t + c_3 h_d + c_4 f_t^2 + c_5 f_t h_d + c_6 h_d^2 \\ & + c_7 f_t^3 + c_8 f_t^2 h_d + c_9 f_t h_d^2 + c_{10} h_d^3, \end{aligned} \tag{23}$$

where c_1–c_{10} are constant parameters that can be estimated by the regressive method from the values of K_n, K_r, and K_t obtained for different cutting conditions. These polynomial models provide a good fit to the specific cutting forces K_n, K_r, and K_t, within the operating range of interest, the percentages of prediction errors of K_n, K_r, and K_t being less than 10%. Once parameters are obtained, the geometric parameters α and λ are employed to calculate the instantaneous chip thickness, cutting area, and cutting force. A flow chart of the entire modeling procedure is given in Fig. 8.

5. Comparison between experimental and numerical results

5.1. Experimental set-up and conditions

The experimental set-up is shown in Fig. 9. The cutting forces were measured using a Kistler 9257B dynamometer and the data were collected by a data-acquisition system. The cutter used was a Nachi high-speed steel ball-end mill. Whilst the workpieces used were T6061, T2024, and T7075 aluminum alloy with hardness values of 55, 77 and 84 HRB (Hardness Rockwell B), respectively.

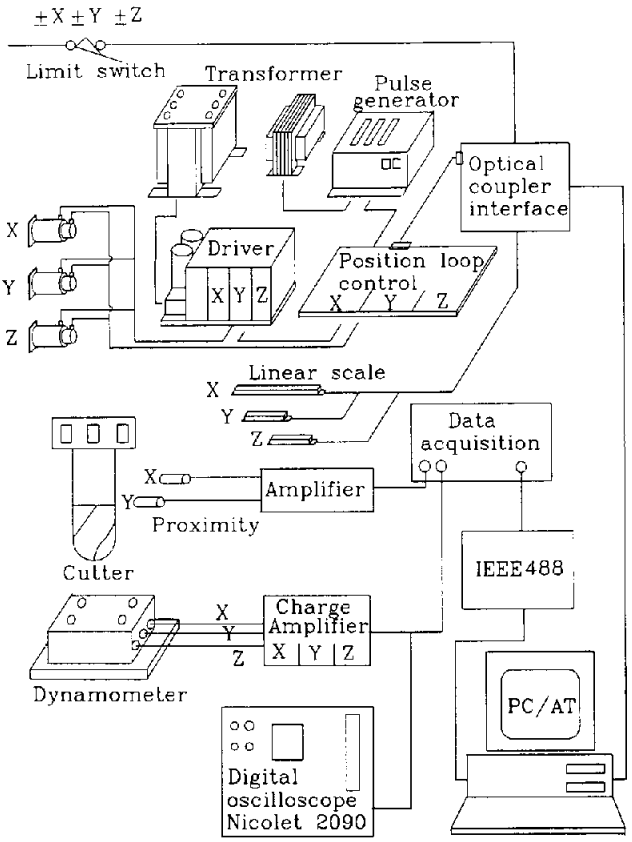

Fig. 9. Experimental set-up.

The experiments consisted of two parts: one part was designed to determine the specific cutting forces and, thus, to obtain the cutting force model; the other part was used to verify the cutting force when the process contains the end-mill part of ball end milling. The cutting conditions for these two parts are listed in Table 2.

5.2. Experimental results and discussion

5.2.1. The relationship between K_n, K_r, K_t and f_t, h_d

The experiments performed to determine K_n, K_r, and K_t were conducted with 180 cutting conditions from the combination of the conditions listed in Table 2. Thus, 180 values of K_n, K_r, and K_t were obtained from Eq. (22). Fig. 10 presents the values obtained for K_n, K_r, and K_t vs. feed per tooth f_t for the workpiece of hardness 84 HRB. From this figure, It is seen that K_n, K_r, and K_t decrease as the feed per tooth increases. It is also noted that the specific cutting force K_t is minimum and the specific cutting force K_n is maximum, amongst the values of K_n, K_r, and K_t.

Table 2
The cutting conditions

Experiments (part 1)	
Cutting conditions	Down milling, $\delta_{A_d} = 0$ Spindle speed: 300, 600, 900 rpm Feedrate: 1, 2, 3, 4, 5 mm/s Hardness: 55, 77, 84 HRB Axial dept of cut: 3, 6 mm Radial depth of cut: 4, 8 mm No coolant
Experiments (part 2)	
Cutting conditions	Down milling, $\delta_{A_d} = 0$ Spindle speed: 900 rpm Feedrate: 1, 2, 3 mm/s Hardness: 55, 77, 84 HRB Axial depth of cut: 12, 16 mm Radial depth of cut: 1, 2, 3 mm No coolant

Table 3
Coefficients of K_n, K_r and K_t

	K_n	K_r	K_t
c_1	-1.140×10^{-3}	-1.800×10^{-3}	-5.100×10^{-4}
c_2	-1.685×10^{4}	-2.850×10^{4}	-1.053×10^{4}
c_3	1.087×10^{2}	1.507×10^{2}	7.204×10^{1}
c_4	1.399×10^{4}	2.059×10^{4}	7.189×10^{3}
c_5	3.977×10^{2}	7.069×10^{2}	2.669×10^{2}
c_6	-2.590×10^{0}	-4.030×10^{0}	-1.958×10^{0}
c_7	-2.955×10^{4}	-4.292×10^{4}	-1.667×10^{4}
c_8	2.023×10^{2}	2.861×10^{2}	1.219×10^{2}
c_9	-3.902×10^{0}	-6.552×10^{0}	-2.535×10^{0}
c_{10}	1.885×10^{-2}	3.059×10^{-2}	1.467×10^{-2}

Fig. 10 also shows the relationship between K_n, K_r, and K_t when $f_t > 0.2$ (mm/tooth),

$$K_r \cong 0.88 K_n,$$

$$K_t \cong 0.50 K_n. \tag{24}$$

This relationship confirming the assumption in [1,2] that there is a linear relationship between K_n, K_r, and K_t. However, when $f_t < 0.2$ (mm/tooth) this assumption is not correct. This error is avoided in the present paper, because K_n, K_r, and K_t have been considered independently of each other.

5.2.2. Comparison between experimental and simulation results for the ball part

After the specific cutting forces are obtained, the cutting force can be predicted by inserting these values into the cutting force model. Some of the predicted and

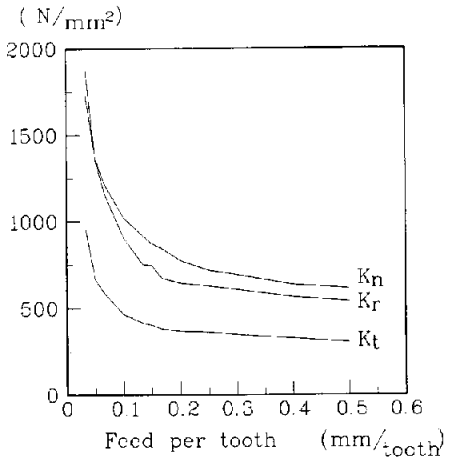

Fig. 10. The specific cutting force K_n, K_r, K_t vs. feed per tooth for the workpiece of hardness HRB = 84.

Table 4
Actual and predicted cutting-forces of the part 1 experiments (radial depth of cut R_d = 4 mm)

No	f_t (mm/tooth)	h_d (HRB)	A_d (mm)	rpm	Measured forces (N)			Predicted forces (N)		
					F_X	F_Y	F_Z	F_X	F_Y	F_Z
1	0.033	55	3	900	18.6	62.6	42.2	15.4	60.1	35.6
2	0.033	77	3	900	17.2	80.5	58.1	16.1	77.7	50.8
3	0.033	84	3	900	24.1	116.6	101.3	19.1	102.6	77.9
4	0.050	55	6	600	24.3	78.8	49.7	22.0	82.1	46.4
5	0.050	77	6	600	24.9	102.0	62.2	22.3	104.9	65.8
6	0.050	84	6	600	31.4	140.6	108.3	26.5	139.6	103.9
7	0.067	55	3	900	16.1	61.9	45.4	16.9	58.1	43.8
8	0.067	77	3	900	16.9	76.1	60.5	17.3	72.1	60.9
9	0.067	84	3	900	17.5	102.3	96.7	22.5	94.3	95.9
10	0.100	55	6	600	20.7	74.3	58.7	23.3	76.0	52.1
11	0.100	77	6	600	16.7	95.0	73.4	22.4	90.7	69.8
12	0.100	84	6	600	19.5	124.7	112.9	29.1	119.1	115.5
13	0.200	55	3	300	47.8	101.6	61.9	42.1	125.2	75.6
14	0.200	77	3	300	31.5	156.4	105.0	34.0	129.4	80.2
15	0.200	84	3	300	31.1	184.5	153.8	42.5	160.7	135.8
16	0.200	55	6	300	69.6	202.5	89.8	70.8	213.0	100.0
17	0.200	77	6	300	75.7	250.4	122.8	69.9	201.0	96.2
18	0.200	84	6	300	85.4	281.9	189.5	82.9	243.9	161.4

experimental cutting forces for the same cutting conditions are listed in Table 4, and one of the cases is shown in Fig. 11. In this latter figure, the trend in the measured and predicted forces is similar in every respect. The results in the table show also that the mean force errors are less than 15% and are thus more accurate than the error of 20% given in [5], which is because in the present work the cutting range is considered more

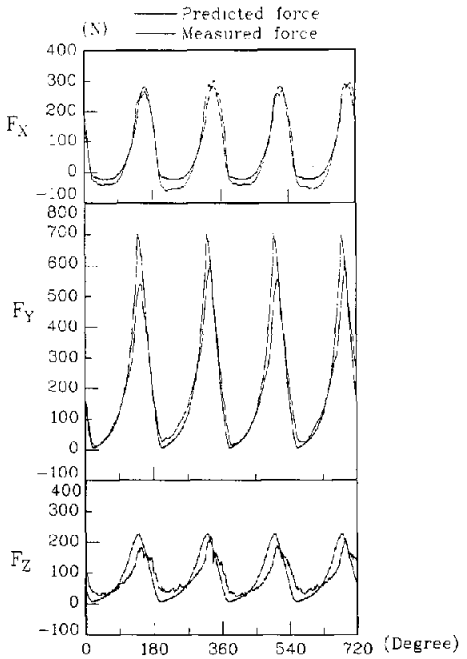

Fig. 11. Comparisons of predicted and actual cutting-forces in the X, Y, and Z directions. (test number 16 of Table 4 with v = 300 rpm, h_d = 55 HRB, A_d = 6 mm, R_d = 4 mm, f_t = 0.2 mm/tooth).

adequately and a more accurate force model is used. The remaining predictive errors can be attributed to the following:

1. Although the assumption that K_n, K_r, and K_t are a third-order function of f_t and h_d is reasonable, a small error still exists.
2. The deflection of the cutter is neglected.
3. There is an error between the actual profile of the edge and the approximate profile.

Because of reason 2, as shown in Fig. 11, the predicted value of the Y direction force at the apogee is greater than the experimental value, since the deflection makes the real radial depth of cut less than the given depth of cut.

5.2.3. Comparison between experimental and simulation results for both the ball and end-mill parts

Selected results on the cutting force for both the ball and the end-mill parts from simulation and experiment are listed in Table 5, and one particular case is shown in Fig. 12. The results show that the error is less than 20%, which is slightly greater than the error described in Section 5.2.2. The error is greater because the rake angle was derived using the model of the ball-end-mill part, which has a bias to the real rake angle of the end-mill part. Thus, the derived coefficients c_1–c_{10} in the specific cutting forces generate an error, which error can be decreased by considering these coefficients separately for the ball part and the end-mill part.

Table 5
Actual and predicted cutting-forces of the part 2 experiments (radial depth of cut R_d = 2 mm and spindle speed v = 900 rpm)

No	f_t (mm/tooth)	h_d (HRB)	A_d (mm)	Measured forces (N)			Predicted forces (N)		
				F_X	F_Y	F_Z	F_X	F_Y	F_Z
1	0.033	55	12	35.9	62.8	27.9	27.7	52.4	17.2
2	0.033	77	12	39.3	72.4	28.6	32.0	72.0	25.3
3	0.033	84	12	45.5	114.7	57.1	39.4	98.0	41.8
4	0.067	55	12	58.0	94.5	37.8	48.9	88.5	24.9
5	0.067	77	12	60.4	102.7	40.0	54.2	114.8	36.3
6	0.067	84	12	67.8	147.5	70.8	66.7	159.8	65.2
7	0.033	55	16	50.2	84.9	26.9	94.8	70.3	14.6
8	0.033	77	16	50.0	86.3	27.8	40.0	93.7	22.3
9	0.033	84	16	52.6	127.4	51.8	48.8	128.6	30.3
10	0.067	55	16	75.1	114.4	31.8	61.6	114.3	19.9
11	0.067	77	16	76.4	123.7	33.9	67.9	148.9	30.4
12	0.067	84	16	83.2	167.7	59.7	82.8	209.3	60.6

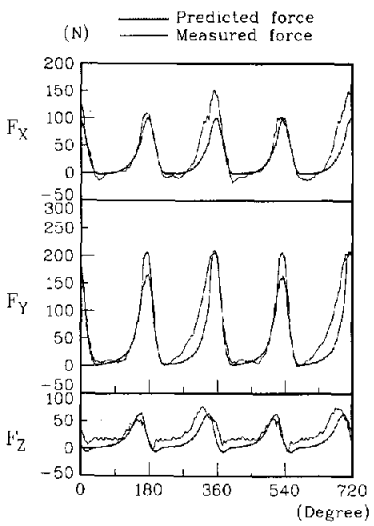

Fig. 12. Comparisons of predicted and actual cutting forces in X, Y, and Z directions. (test number 1 of Table 5 with v = 900 rpm, h_d = 55 HRB, A_d = 12 mm, R_d = 2 mm, f_t = 0.033 mm/tooth).

6. Conclusions

This paper develops a method for predicting the cutting force in ball-end milling. The method is simple and yields a more accurate cutting-force model, attributed to the following: (i) a correct description of the cutting edge; (ii) complete cutting

boundary conditions; and (iii) an adequate transformation of the infinitesimal cutting force.

The results of the simulations and experiments reported here support the following conclusions:

1. If the axial depth of cut is greater than the radius of the cutter, the cutting force can still be predicted using the proposed cutting-force model.
2. In the proposed method, the slope of the edge is approximated in the end mill part by the angle λ_e instead of the saw-tooth approximation. Using the angle λ_e results in far less bias of profile fitting and thus in a much lesser prediction error.
3. The appropriate range of entry angle β_{en} due to the cusp effect is considered in this paper and a more accurate cutting range is given, i.e., the cutting force is estimated much more accurately.

References

[1] J. Tlusty and P. Macneil, Dynamics of cutting forces in end milling, Ann. CIRP 24, (1975), 20–25.
[2] W.A. Kline, R.E. Devor and J.R. Lingberg, The prediction of cutting forces in end milling with application to cornering cuts, *Int. J. Mach. Tool Des. Res.*, 22(1) (1982) 7–22.
[3] W.A. Kline and R.E. Devor, The effect of runout of cutting geometry and forces in end milling, *Int. J. Mach. Tool Des. Res.*, 23(2/3) (1983) 123–140.
[4] Y. Fujii and T. Terai, Ball-nose end mills simulator – Simulation of a cutting force, *J. Japan Soc. Prec. Eng.* (in Japanese), 54(12) (1988) 2301–2306.
[5] M. Yang and H.D. Park, The prediction of cutting forces in ball end milling, *Int. J. Mach. Tool Manuf.*, 31(1) (1991) 45–54.
[6] A. Hirota and E. Usui, Analytical prediction of cutting forces in slab milling operation, *Bull. Japan Soc. Prec. Eng.*, 15(1) (1981) 40–46.